

Improved analytical fit of gold dispersion: Application to the modeling of extinction spectra with a finite-difference time-domain method

Alexandre Vial,* Anne-Sophie Grimault, Demetrio Macías, Dominique Barchiesi, and Marc Lamy de la Chapelle
*Laboratoire de Nanotechnologie et d'Instrumentation Optique - CNRS FRE 2671, Université de Technologie de Troyes,
 12 rue Marie Curie, BP-2060 F-10010 Troyes Cedex, France*

(Received 13 July 2004; revised manuscript received 14 October 2004; published 23 February 2005)

We propose an accurate description for the dispersion of gold in the range of 1.24–2.48 eV. We implement this improved model in an FDTD algorithm and evaluate its efficiency by comparison with an analytical method. Extinction spectra of gold nanoparticle arrays are then calculated.

DOI: 10.1103/PhysRevB.71.085416

PACS number(s): 41.20.Jb, 42.25.Bs, 77.22.Ch, 78.20.Ci

I. INTRODUCTION

The employment of the finite-difference time-domain (FDTD) method in the study of different electromagnetic phenomena has raised constantly increasing interest over the past 15 years. Since then, an extensive number of references describing the principles of the method have been published; see, e.g., Refs. 1 and 2. Also, a wide variety of software based on this technique has been developed and is commercially, and noncommercially, available elsewhere.

Due to the fact that accurate results for a full spectrum can be obtained in a single run of the program, the FDTD has proven to be well adapted for different kinds of spectroscopic studies.³ Nevertheless, a strong limitation is the requirement of an analytical model of dispersion. Typical laws used for FDTD simulations are the Debye, Lorentz, or Drude dispersion models.^{3–6} Also, a modified Debye law can be used.⁷ At least in principle, any dispersion law could be described in terms of a linear combination of Debye and Lorentz laws.² Surprisingly, this property has not been used in studies using the FDTD method. Rather, it has been successfully applied to the description of optical functions for 11 metals over a wide spectrum,⁸ or to a calculation of the reflectance of single wall nanotubes.⁹ In this paper, we will employ a scheme similar to the one that appears in this last reference for the study of the optical response of gold nanostructures.

The structure of this work is as follows. In Sec. II, we show the results obtained from the implementation of two classic dispersion models employing the FDTD method. In order to validate the numerical approaches, we apply them to the case of a simple structure and compare the results with those obtained using the analytical method described in Ref. 10. In Sec. III, we employ our FDTD-based implementation of the Drude-Lorentz model to the calculation of extinction spectra. In Sec. IV, we present our main conclusions and final remarks.

II. MODELS OF DISPERSION

A. The Drude model

It is well known that in the near infrared, the relative permittivity of several metals can be described by means of the Drude model,¹¹

$$\epsilon_D(\omega) = \epsilon_\infty - \frac{\omega_D^2}{\omega(\omega + i\gamma_D)}, \quad (1)$$

where ω_D is the plasma frequency and γ_D is the damping coefficient. Nevertheless, if frequencies within the range of the visible spectrum are required for a specific study, the model in Eq. (1) may not be complete enough to provide accurate results. To illustrate this fact, we try to fit the relative permittivity of gold ϵ_{JC} , tabulated by Johnson and Christy¹² through the optimization of ϵ_∞ , ω_D , and γ_D for energies between 1.24 and 2.48 eV (wavelengths between 500 and 1000 nm). In order to determine the best set of parameters, we define a fitness function (sometimes called an objective function) Φ as

$$\Phi = \sum_{\omega_j} \{ \text{Re}[\epsilon_{JC}(\omega_j) - \epsilon_D(\omega_j)] \}^2 + \{ \text{Im}[\epsilon_{JC}(\omega_j) - \epsilon_D(\omega_j)] \}^2, \quad (2)$$

where ω_j are the discrete values of the frequency $\omega = 2\pi c/\lambda$ for which the permittivity is calculated. The real and imaginary parts of a complex value z are, respectively, $\text{Re}(z)$ and $\text{Im}(z)$. The minimization of Φ is performed employing the simulated annealing procedure described in Ref. 13, and results are presented in the first row of Table I.

The real and imaginary parts of the permittivity $\epsilon_D(\omega)$, calculated with the Drude model, are, respectively, plotted with a dotted line in Figs. 1 and 2.

It can be seen that neither $\text{Re}(\epsilon_{JC})$ nor $\text{Im}(\epsilon_{JC})$ are well described for energies above 2.2 and 1.9 eV, respectively. To emphasize this difference, we also plot in Figs. 1 and 2 the relative errors on $\text{Re}(\epsilon_D)$ and $\text{Im}(\epsilon_D)$. The existence of a strong discrepancy for energies above 1.9 eV when using the single Drude model is evident.

Due to the inability of the Drude model to describe the permittivity of metals over a wide range of frequencies, some of the authors working with the FDTD restrict their studies to a zone of the spectrum where the Drude model is valid (Ref. 7 for a gold tip, Refs. 14 and 15 for silver and aluminum structures; it should be noted that for these two metals, the Drude model alone works well for the optical wavelengths). Others try to fit the permittivity in the range of interest by modifying the values of the parameters ϵ_∞ , ω_D , and γ_D of the model, as shown in Ref. 5 for the case of silver

TABLE I. Values of the parameters used for the optimization of the Drude and the Drude-Lorentz models. The value of the fitness function is given in the last column.

	ϵ_∞	$\omega_D/2\pi$ (THz)	$\gamma_D/2\pi$ (THz)	$\Omega_L/2\pi$ (THz)	$\Gamma_L/2\pi$ (THz)	$\Delta\epsilon$	Φ
Drude	9.0685	2155.6	18.36				431.46
Drude-Lorentz	5.9673	2113.6	15.92	650.07	104.86	1.09	14.521

structures or in Ref. 15 for a gold nanostructure. In this last reference, Drude parameters are actually adapted for several particular wavelengths.

One way to overcome the limitations of the Drude model could be to split the spectrum in several zones and use a different set of parameters for each of these parts in order to get the best fit. However, a drawback of this solution is that a whole new computation is required for each set of parameters.

B. Extended Drude model

Another way to overcome the limitations of the Drude model for gold in the 1.24–2.48 eV range, and also to take into account the interband transitions, is suggested in Ref. 11. It consists in the addition of one or several Lorentzian terms to Eq. (1). This approach was used in Ref. 8, where five Lorentzian terms were added in order to fit the permittivity of 11 metals for energies between 0.1 and 5 eV. Nevertheless, as the authors acknowledge themselves, the Drude-Lorentz model does not fit very well experimental values around 2 eV for gold, even with additional terms. Moreover, we aim to implement our improved dispersion law in an FDTD code, and the memory requirements increase linearly with the number of terms used for the dispersion law. For these reasons, we decided to restrict our model of dispersion to only one additional Lorentzian term. Thus, we write the permittivity of gold as

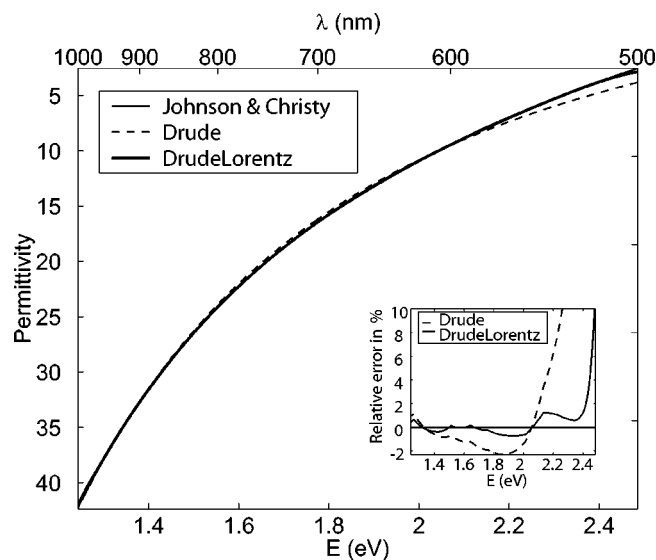


FIG. 1. Real part of the permittivity of gold as published in Ref. 12, calculated with the single Drude model and calculated with the Drude-Lorentz model.

$$\epsilon_{DL}(\omega) = \epsilon_\infty - \frac{\omega_D^2}{\omega(\omega + i\gamma_D)} - \frac{\Delta\epsilon \cdot \Omega_L^2}{(\omega^2 - \Omega_L^2) + i\Gamma_L\omega}, \quad (3)$$

where Ω_L and Γ_L , respectively, stand for the oscillator strength and the spectral width of the Lorentz oscillators, and $\Delta\epsilon$ can be interpreted as a weighting factor.

In order to find the best set of parameters and the best fit of $\epsilon_{JC}(\omega)$, we employ the same optimization scheme as we did for the Drude model. The new parameters are presented in the second row of Table I.

In order to facilitate the comparison with the results obtained employing the single Drude model, we depict with a solid line in Figs. 1 and 2 the real and imaginary parts calculated with the Drude-Lorentz model. The agreement between the experimental values and the ones described by Eq. (3) is quite good for the whole spectrum. The initial discrepancies present for energies above 1.9 eV, when using the Drude model, have been removed. This effect is illustrated further when we plot the relative errors on $\text{Re}(\epsilon_{DL})$ and $\text{Im}(\epsilon_{DL})$.

The improved law of dispersion in Eq. (3) is now implemented in our FDTD code through the recursive convolution method described in Ref. 1 for validation. Details on the numerical implementation are given in an Appendix at the end of this paper.

C. Validation of the new approach

In order to evaluate the performance of our approach, we will compare its results with those obtained employing an

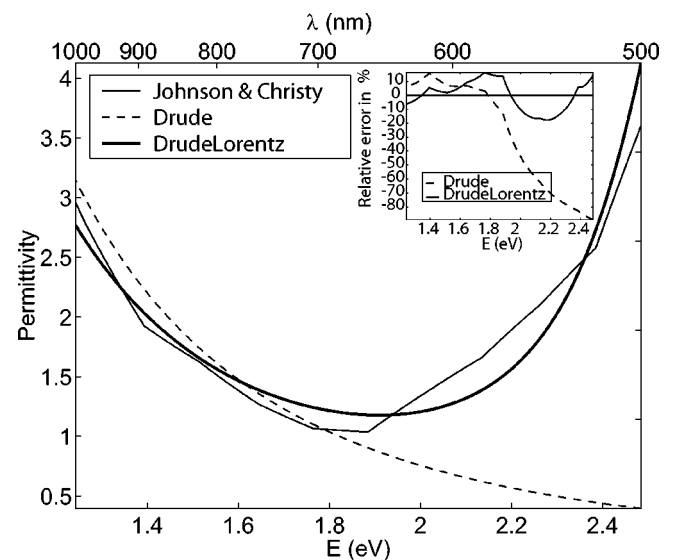


FIG. 2. Imaginary part of the permittivity of gold as published in Ref. 12, calculated with the single Drude model and calculated with the Drude-Lorentz model.

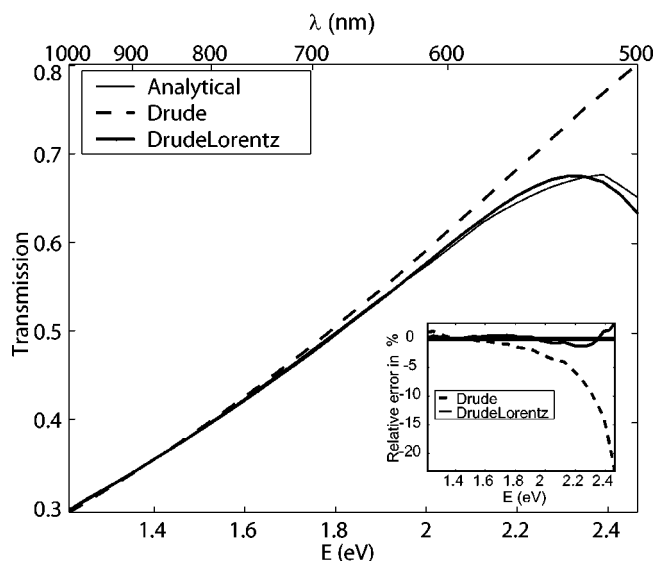


FIG. 3. Coefficient of transmission through a layer of 20 nm of gold, respectively, calculated analytically, with the simple Drude model and with the Drude-Lorentz model. The relative error on $|t|$ by comparison with the analytical result is also depicted.

analytical method. For simplicity, the structure we will consider for our tests consists of a thin layer of gold surrounded by air. We will calculate the coefficient of transmission in amplitude for the electric field using the formulas that appear in Ref. 10 for an absorbing film on a transparent substrate.

In Fig. 3, we present the results obtained considering a thin film of thickness $e=20$ nm. The absolute values of the transmission coefficients $|t|$, computed through the FDTD implementations of Drude and Drude-Lorentz models, are, respectively, depicted with a dashed and a thick solid curve. The thin solid curve corresponds to the analytical result. The values of the permittivity used for the analytical calculation are the ones published in Ref. 12 and not the values fitted by the Drude-Lorentz model.

It can be observed in Fig. 3 that the agreement between the Drude model and the analytical one decreases for energies above 1.8 eV (wavelength below 700 nm). On the other hand, the agreement between the Drude-Lorentz model and the analytical one is quite good. This behavior can be visualized further by plotting the relative error on the values of $|t|$ for the two models used with the FDTD method. It is obvious from Fig. 3 that the Drude-Lorentz model not only performs better than the Drude model, but also that it leads to a very small error on a wide spectrum. The maximal relative error obtained with the Drude-Lorentz model is 2.7%, and if we consider this value as a threshold for the validity of the model, the Drude model is only valid for energies below 1.97 eV (wavelengths greater than 630 nm).

According to Figs. 1 and 2, it is clear that the imaginary part of the permittivity is less well described than the real one even with the Drude-Lorentz model, thus we can check results obtained for $|t|$ when considering a layer of thickness $e=50$ nm (Fig. 4) in order to verify that we still get satisfying results. It can be seen that both the transmission coefficients $|t|$ and the relative errors present a behavior analogous to the one shown in Fig. 3, and similar conclusions can be

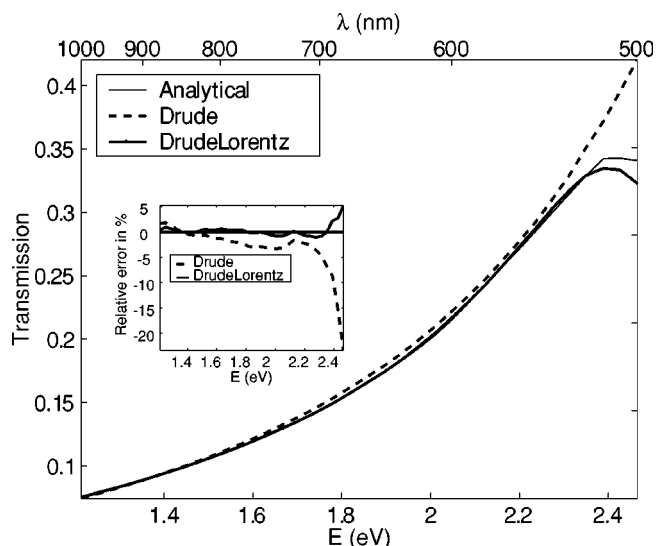


FIG. 4. Coefficient of transmission through a layer of 50 nm of gold, respectively, calculated analytically, with the simple Drude model and with the Drude-Lorentz model. The relative error on $|t|$ by comparison with the analytical result is also depicted.

drawn. In this case, the maximal error achieved when using the Drude-Lorentz model is 5.2%, and the Drude model performs worse only for energies above 2.34 eV (wavelengths below 530 nm). If now we still consider the threshold previously defined (maximal error of 2.7%), then the Drude-Lorentz model can be accepted for energies below 2.39 eV (wavelengths greater than 520 nm), whereas the Drude model is only acceptable for energies below 1.78 eV (wavelengths above 697 nm) and in a narrow zone between 2.08 and 2.24 eV (555 and 596 nm).

As a last test, we compute the intensity 5 nm above an infinite gold cylinder of radius 15 nm illuminated with a plane wave, the incident field being polarized perpendicularly with the axis of the cylinder. Results are compared with the Mie theory and presented in Fig. 5. It is confirmed that the Drude-Lorentz models perform better than the single Drude model, which is unable to predict the peak of absorption around 2.4 eV. Nevertheless, the error calculated in this case is higher than previously observed, mainly due to the difficulty to accurately describe a circle using an orthogonal mesh. For this calculation, in order to refine the description of the shape of the cylinder, a spatial discretization of 0.5 nm was used, instead of 5 nm for the thin-layer cases.

Once we have verified that an improvement can be observed not only on the description of the permittivity ϵ , but also on the calculation of transmission coefficients, we feel confident to apply our new dispersion model to a more complicated case, namely the calculation of extinction spectra above gold nanostructures arrays.

III. APPLICATION TO THE CALCULATION OF EXTINCTION SPECTRA

Recently, several experimental results obtained with gold nanoparticle arrays have been published.¹⁶⁻²¹ Various sizes,

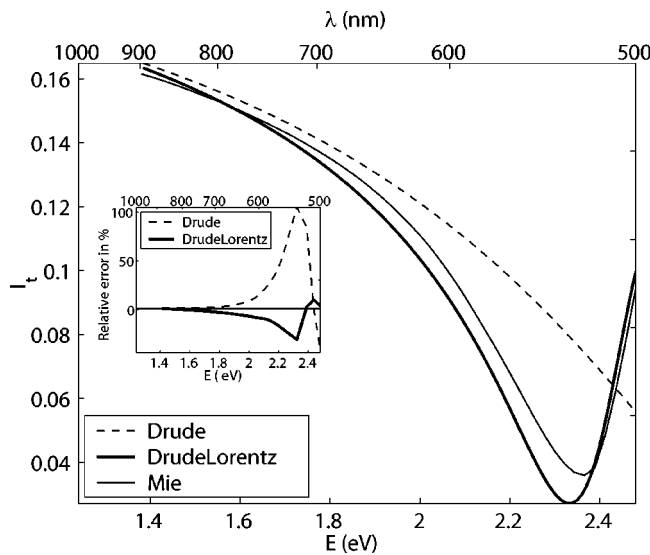


FIG. 5. Intensity transmitted above a gold cylinder of radius 15 nm, respectively, calculated analytically (Mie theory), with the simple Drude model and with the Drude-Lorentz model. The relative error by comparison with the analytical result is also depicted.

shapes, and periodicities are used in order to tune the position of the extinction, and the influence of these parameters was reviewed in Ref. 22. These experiments are mainly focused on the development and the improvement of surface enhanced Raman spectroscopy (SERS) active substrate.

In this section, we will present computations of extinction spectra on two kinds of gold nanoparticle arrays. As most of the figures published in previously cited papers show the spectra as a function of the wavelength, the following figures will maintain the same convention.

A. Geometry of the problem

The typical shape of the structures used for SERS experiments is depicted in Fig. 6. It consists of a substrate made of glass on which gold nanoparticles are deposited. For our forthcoming calculations, the incident field is assumed to be a plane wave with a Gaussian temporal shape. The sample is

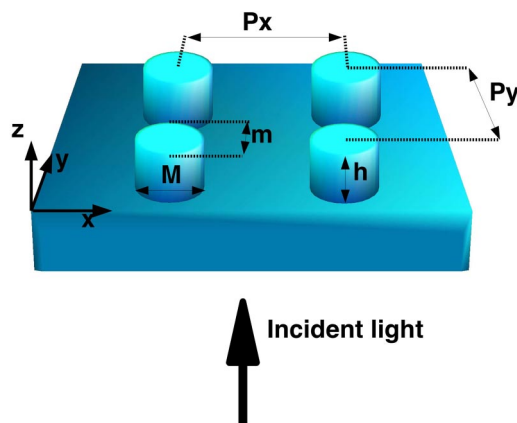


FIG. 6. Geometry of the structure studied for the calculation of the extinction spectrum.

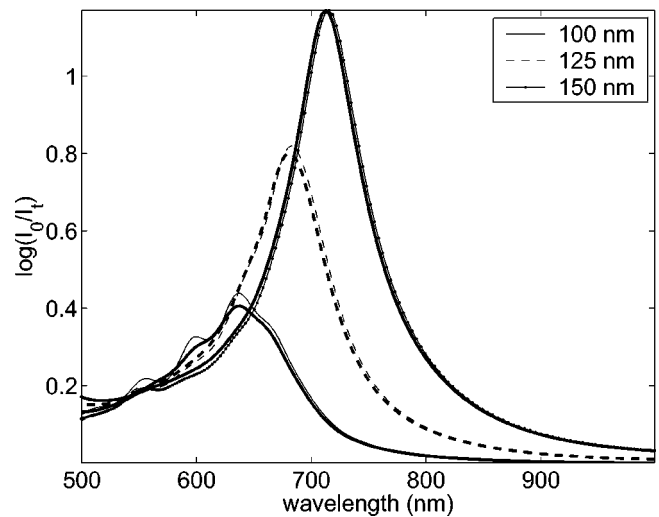


FIG. 7. Extinction spectra calculated for gold cylinders with an elliptical basis: the height is 60 nm, the grating constant is 300 nm, and the major and minor axes are, respectively, 100 nm and 100 nm (structure A), 125 nm and 100 nm (structure B), and 150 nm and 100 nm (structure C). Calculations performed with the Drude-Lorentz model are depicted with a thick line. Calculations performed with the Drude model are depicted with a thin line. Peak positions for structures A, B, and C are, respectively, $\lambda=637$ nm, $\lambda=680$ nm, and $\lambda=712$ nm with the Drude-Lorentz model, and $\lambda=637$ nm, $\lambda=683$ nm, and $\lambda=715$ nm for the Drude model.

illuminated from the $z < 0$ region at normal incidence. The value of the electric field is recorded after each time step of the calculation on a plane above the particles. Once we have checked that the Gaussian pulse has vanished and that no electric field remains in the computing window, we stop the computation, and it is then straightforward to calculate the extinction spectrum of the structure by performing a Fourier transform of the field.^{1,2} The results presented in the following subsections are computed with spatial discretization $\Delta x = 5$ nm, and the time step Δt is defined as $\Delta t = \Delta x / (2c)$ with c the speed of light in vacuum.

B. Numerical results

In the first case, the particles in Fig. 6 are cylinders with an elliptical basis and a height of 60 nm. One of the axes of the ellipse has a constant length ($m=100$ nm), whereas the length of the second axis is variable (structure A: $M=100$ nm; structure B: $M=125$ nm; structure C: $M=150$ nm). The periodicity of the array along the x and y directions is $p_x = p_y = 300$ nm. The incident light is polarized along the x axis. The extinction spectra obtained for structures A, B, and C are plotted in Fig. 7 with thick solid or dashed curves.

These results are in good agreement with those published in Ref. 20, where increasing the size of the major axis of the ellipse induced a strong redshift of the peak. Results obtained with the Drude model are also depicted in Fig. 7 with thin solid or dashed lines. It can be observed that the positions of the peaks are almost the same, but oscillations are

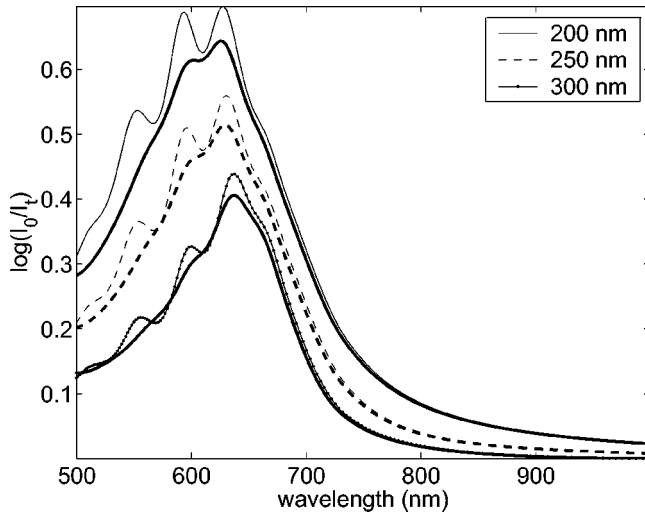


FIG. 8. Extinction spectra calculated for gold cylinders: the height is 60 nm, the diameter is 100 nm, and grating constants are, respectively, 200 nm (structure A), 250 nm (structure B), and 300 nm (structure C). Calculations performed with the Drude-Lorentz model are depicted with a thick line. Calculations performed with the Drude model are depicted with a thin line. Peak positions for structures A, B, and C are, respectively, $\lambda=625$ nm, $\lambda=630$ nm, and $\lambda=638$ nm with the Drude-Lorentz model, and $\lambda=628$ nm, $\lambda=630$ nm, and $\lambda=638$ nm for the Drude model.

present on the spectrum calculated with the Drude model for structure A.

In the second case, particles are cylinders with a diameter of 100 nm and a height of 60 nm, and the periodicity of the array is changed (structure A: $p_x=p_y=200$ nm; structure B: $p_x=p_y=250$ nm; structure C: $p_x=p_y=300$ nm). Results are presented in Fig. 8 with thick solid or dashed lines.

The behavior of the curves in Fig. 8 is consistent with that of the experimental results published in Ref. 17, where a small shift to the red was observed when increasing the period of the grating. Moreover, our model gives better results

than the discrete dipole approximation (DDA) used in Ref. 17, as it gives the right direction for the shift of the peak.

The benefit of using Eq. (2) instead of the standard Drude model given in Eq. (1) can be seen by comparing results obtained with the single Drude model depicted with thin lines in Fig. 8. Positions of the peaks are still almost the same, but strong oscillations are present on the left part of the spectrum for all structures.

IV. CONCLUSION

By adding a Lorentzian term to the widely used Drude model, we were able to fit the dispersion curve of gold over a spectrum wider than possible with the single Drude model. This improved dispersion law was then implemented in a FDTD code and applied to the calculation of gold nanoparticle arrays extinction spectra. Calculations are in good agreement with experimental results. When calculations are made with the original Drude model, only a small shift of the absorption peak may be observed for some structures, but strong oscillations in the spectrum are visible for wavelengths below the resonance. This behavior is an indication that intensities calculated above or inside the metallic structure would then be wrong, leading to inexact estimations of the SERS gain.

Further work is still required in order to be able to fit the permittivity of gold over the full visible spectrum. This could be achieved by adding at least one more Lorentzian term. Moreover, other metals often used for the design of nanostructures, like silver or aluminum, should be studied too.

ACKNOWLEDGMENTS

D.M. acknowledges Le Ministère de la Jeunesse, de l'Éducation Nationale et de la Recherche as well as the Conseil Régional de Champagne-Ardennes for financial support. A.-S. Grimault acknowledges the Conseil Régional de Champagne-Ardennes for financial support.

APPENDIX: 3D NUMERICAL IMPLEMENTATION OF THE DRUDE-LORENTZ MODEL

For a three-dimensional computation window, with a spatial discretization Δx and a temporal discretization Δt , we represent the value of any field U at position $x=i\Delta x$, $y=j\Delta x$, $z=k\Delta x$ and for the instant $t=n\Delta t$ by $U_{i,j,k}^n$, and the standard recursion equations in a nondispersive and nonmagnetic medium for the electric and magnetic fields are

$$H_x|_{i-1/2,j+1,k+1}^{n+1/2} = H_x|_{i-1/2,j+1,k+1}^{n-1/2} + \frac{\Delta t}{\mu_0 \Delta x} (E_y|_{i-1/2,j+1,k+3/2}^n - E_y|_{i-1/2,j+1,k+1/2}^n + E_z|_{i-1/2,j+1/2,k+1}^n - E_z|_{i-1/2,j+3/2,k+1}^n), \quad (\text{A1})$$

$$H_y|_{i,j+1/2,k+1}^{n+1/2} = H_y|_{i,j+1/2,k+1}^{n-1/2} + \frac{\Delta t}{\mu_0 \Delta x} (E_z|_{i+1/2,j+1/2,k+1}^n - E_z|_{i-1/2,j+1/2,k+1}^n + E_x|_{i,j+1/2,k+1/2}^n - E_x|_{i,j+1/2,k+3/2}^n), \quad (\text{A2})$$

$$H_z|_{i,j+1,k+1/2}^{n+1/2} = H_z|_{i,j+1,k+1/2}^{n-1/2} + \frac{\Delta t}{\mu_0 \Delta x} (E_x|_{i,j+3/2,k+1/2}^n - E_x|_{i,j+1/2,k+1/2}^n + E_y|_{i-1/2,j+1,k+1/2}^n - E_y|_{i+1/2,j+1,k+1/2}^n), \quad (\text{A3})$$

$$E_x|_{i,j+1/2,k+1/2}^{n+1} = E_x|_{i,j+1/2,k+1/2}^n + \frac{\Delta t}{\epsilon_0 \epsilon_{i,j+1/2,k+1/2} \Delta x} (H_z|_{i,j+1,k+1/2}^{n+1/2} - H_z|_{i,j,k+1/2}^{n+1/2} + H_y|_{i,j+1/2,k}^{n+1/2} - H_y|_{i,j+1/2,k+1}^{n+1/2}), \quad (\text{A4})$$

$$E_y|_{i-1/2,j+1,k+1/2}^{n+1} = E_y|_{i-1/2,j+1,k+1/2}^n + \frac{\Delta t}{\epsilon_0 \epsilon_{i-1/2,j+1,k+1/2} \Delta x} (H_x|_{i-1/2,j+1,k+1}^{n+1/2} - H_x|_{i-1/2,j+1,k}^{n+1/2} + H_z|_{i-1,+1,j,k+1/2}^{n+1/2} - H_z|_{i,j+1,k+1/2}^{n+1/2}), \quad (\text{A5})$$

$$E_z|_{i-1/2,j+1/2,k+1}^{n+1} = E_z|_{i-1/2,j+1/2,k+1}^n + \frac{\Delta t}{\epsilon_0 \epsilon_{i-1/2,j+1/2,k+1} \Delta x} (H_y|_{i,j+1/2,k+1}^{n+1/2} - H_y|_{i-1,j+1/2,k+1}^{n+1/2} + H_x|_{i-1/2,j,k+1}^{n+1/2} - H_x|_{i-1/2,j+1,k+1}^{n+1/2}). \quad (\text{A6})$$

For a dispersive medium whose dispersion is described by Eq. (3), we need to introduce two new vector fields Ψ_D and Ψ_L known as “recursive accumulators” and Eqs. (A4)–(A6) have to be replaced by the following three equations:

$$\Psi_D|_i^n = C_D^p \Psi_D|_i^{n-1} + C_D^\delta \mathbf{E}|_i^n, \quad (\text{A7})$$

$$\Psi_L|_i^n = C_L^p \Psi_L|_i^{n-1} + C_L^\delta \mathbf{E}|_i^n, \quad (\text{A8})$$

$$\mathbf{E}|_i^{n+1} = C^\alpha \mathbf{E}|_i^n + C^\beta \nabla \times \mathbf{H}^{n+1/2} + C^\gamma \text{Re}(\Psi_D|_i^n + \Psi_L|_i^n), \quad (\text{A9})$$

where the coefficients C^α , C^β , C^γ , C^δ , and C^p depend on the coefficients of Eq. (3).

For the Drude term, we define $\delta_\epsilon = -(\omega_D/\gamma_D)^2$, $\chi_D^0 = \delta_\epsilon(1 - e^{-\gamma_D \Delta t})$, $\Delta \chi_D^0 = \delta_\epsilon(1 - e^{-\gamma_D \Delta t})^2$, and $\sigma_D = \omega_D^2/\gamma_D$. Then the coefficients C_D^p and C_D^δ are defined as

$$C_D^p = e^{-\gamma_D \Delta t}, \quad (\text{A10})$$

$$C_D^\delta = \Delta \chi_D^0. \quad (\text{A11})$$

For the Lorentz term, we first define $\alpha = \Gamma_L/2$, $\beta = \sqrt{\Omega_L^2 - \alpha^2}$, and $\gamma = \Delta \epsilon \Omega_L^2/\beta$. Then we define

$$\chi_L^0 = -i \frac{\gamma}{\alpha - i\beta} (1 - e^{(-\alpha+i\beta)\Delta t}), \quad (\text{A12})$$

$$\Delta \chi_L^0 = -i \frac{\gamma}{\alpha - i\beta} (1 - e^{(-\alpha+i\beta)\Delta t})^2. \quad (\text{A13})$$

Coefficients C_L^p and C_L^δ can now be written as

$$C_L^p = e^{(-\alpha+i\beta)\Delta t}, \quad (\text{A14})$$

$$C_L^\delta = \Delta \chi_L^0. \quad (\text{A15})$$

Finally, we define $\chi^0 = \chi_D^0 + \text{Re}(\chi_L^0)$, and the last three coefficients needed are

$$C^\alpha = \frac{\epsilon_\infty}{\epsilon_\infty + \chi_0 + \sigma_D \Delta t}, \quad (\text{A16})$$

$$C^\beta = \frac{\Delta t}{\Delta x \epsilon_0 (\epsilon_\infty + \chi_0 + \sigma_D \Delta t)}, \quad (\text{A17})$$

$$C^\gamma = \frac{1}{\epsilon_\infty + \chi_0 + \sigma_D \Delta t}. \quad (\text{A18})$$

*Electronic address: alexandre.vial@utt.fr

¹K. Kunz and R. Luebbers, *The Finite Difference Time Domain Method for Electromagnetics* (CRC Press, Boca Raton, FL, 1993).

²A. Taflov and S. Hagness, *Computational Electrodynamics: The Finite-Difference Time-Domain Method* (Artech House, Boston, 2000).

³M. Beard and C. Schmittenmaer, *J. Chem. Phys.* **114**, 2903 (2001).

⁴F. Teixeira, W. C. Chew, M. Straka, M. Oristaglio, and T. Wang, *IEEE Trans. Geosci. Remote Sens.* **36**, 1928 (1998).

⁵S. K. Gray and T. Kupka, *Phys. Rev. B* **68**, 045415 (2003).

⁶M. Futamata, Y. Maruyama, and M. Ishikawa, *J. Phys. Chem. B* **107**, 7607 (2003).

⁷J. T. K. II, E. J. Sanchez, and X. S. Xie, *J. Chem. Phys.* **116**, 10895 (2002).

⁸A. Rakić, A. Djurisić, J. Elazar, and M. Majewski, *Appl. Opt.* **37**, 5271 (1998).

⁹A. Ugawa, A. Rinzler, and D. Tanner, *Phys. Rev. B* **60**, R11 305

(1999).

¹⁰M. Born and E. Wolf, *Principle of Optics*, 6th ed. (Pergamon Press, Oxford, 1980).

¹¹C. Bohren and D. Huffman, *Absorption and Scattering of Light by Small Particles* (Wiley, New York, 1983).

¹²P. Johnson and R. Christy, *Phys. Rev. B* **6**, 4370 (1972).

¹³S. Kirkpatrick, C. D. Gelatt, and M. P. Vecchi, *Science* **220**, 671 (1983).

¹⁴F. I. Baida and D. Van Labeke, *Opt. Commun.* **209**, 17 (2002).

¹⁵F. I. Baida, D. Van Labeke, and Y. Pagani, *Opt. Commun.* **225**, 241 (2003).

¹⁶S. Linden, J. Kuhl, and H. Giessen, *Phys. Rev. Lett.* **86**, 4688 (2001).

¹⁷N. Félidj, J. Aubard, G. Lévi, J. Krenn, M. Salerno, G. Schider, B. Lamprecht, A. Leitner, and F. Aussenegg, *Phys. Rev. B* **65**, 075419 (2002).

¹⁸N. Félidj, J. Aubard, G. Lévi, J. Krenn, G. Schider, A. Leitner, and F. Aussenegg, *Phys. Rev. B* **66**, 245407 (2002).

¹⁹N. Félidj, J. Aubard, G. Lévi, J. Krenn, A. Hohenau, G. Schider,

- A. Leitner, and F. Aussenegg, *Appl. Phys. Lett.* **82**, 3095 (2003).
- ²⁰J. Grand, S. Kostcheev, J.-L. Bijeon, M. L. D. L. Chapelle, P.-M. Adam, A. Rumyantseva, G. Lrondel, and P. Royer, *Synth. Met.* **139**, 621 (2003).
- ²¹N. Félidj, S. Truong, G. Lévi, J. Krenn, A. Hohenau, A. Leitner, and F. Aussenegg, *J. Chem. Phys.* **120**, 7141 (2004).
- ²²K. Kelly, E. Coronado, L. L. Zhao, and G. C. Schatz, *J. Phys. Chem. B* **107**, 668 (2003).